

## A polarization in an exact rotating and expanding fluid dynamical model for peripheral heavy ion reactions

Yilong Xie, Robert C. Glastad, and László P. Csernai

*Institute of Physics and Technology, University of Bergen, Allegaten 55, N-5007 Bergen, Norway*

(Received 28 July 2015; revised manuscript received 12 October 2015; published 2 December 2015)

We calculate the A polarization in an exact analytical, rotating model based on parameters extracted from a high resolution (3+1)D particle-in-cell relativistic hydrodynamics calculation. The polarization is attributed to effects from thermal vorticity and for the first time the effects of the radial and axial acceleration are also studied separately.

DOI: 10.1103/PhysRevC.92.064901

PACS number(s): 25.75.-q, 24.70.+s, 47.32.Ef

### I. INTRODUCTION

In high energy peripheral heavy ion collisions there is a substantial amount of initial angular momentum directly after the Lorentz contracted nuclei penetrate each other. The formed quark gluon plasma locally equilibrates, the shear flow leads to local rotation, i.e., vorticity, and then it expands, while its rotation slows down.

Because of the finite impact parameter, the initial stages (IS) have a nonvanishing angular momentum [1,2]. For the initial stages, effective models such as the color glass condensate (CGC) or Glauber model are used. In general, we use experimental data, to construct a possible IS, at a given impact parameter for the participant nucleons, and their eccentricity. Early studies neglected effects arising from the nonvanishing angular momentum, but interest increased recently [3–6].

After many decades of refinements [7,8], hydrodynamical modeling became the best to describe the middle stages of heavy ion collisions at relativistic energies. Thus, rotation and its consequences in peripheral collisions were also studied in fluid dynamical models [9,10].

We look at polarization in effects arising from thermal vorticity in the exact rotating and expanding model [11], where we are modeling an appropriate time period of the collision [12]. Special attention was given to the collective motion, and to extract it from observables which could confirm that such descriptions are indeed plausible.

We calibrate an exact rotating model based on a (3+1)D fluid dynamical model, the relativistic particle-in-cell method (PICR), to fine tune the initial parameters of the rotating and expanding fireball [12].

In Ref. [13] the differential Hanbury Brown and Twiss (HBT) method was used to detect rotation in heavy ion collisions.

Without at least some viscosity and/or interaction one could not generate rotation from the original shear flow. On the other hand to develop instabilities or turbulence the viscosity should be small, so that the ratio of shear viscosity to entropy density  $\eta/s$  should be of the order of  $\hbar/4\pi k_B$ , which can be achieved at the phase transition between hadronic matter and QGP [14].

Thermal vorticity arises from the flow velocity field [15], and the inverse temperature field present in heavy ion collisions, and it arises mainly from a nonvanishing angular momentum in the initial stage.

Fluctuations in the transverse plane can generate significant vorticity, but in peripheral collisions the initial shear flow leads to an order of magnitude larger vorticity [15]. This vorticity may be further enhanced by the Kelvin-Helmholtz instability (KHI).

In our formalism, the dynamics of the system after local equilibration is computed using the relativistic (3+1)D fluid dynamical model PICR. This fluid dynamical (FD) computation with small viscosity shows enhanced collective rotation from an evolving KHI. In Ref. [16] a simple analytic model for this phenomenon is explored using a few material properties: the surface tension between the colliding nuclei, the viscosity, and the thickness of the flow layer. This enables a classical potential flow approximation, in which one may study the dynamics of an onsetting KHI.

A more recent calculation of the onset and effects of the KHI is performed in Ref. [12], in which the calibration of the “Exact” model takes place. Here, it is pointed out that this feature—the enhancement of rotation—is a dominant aspect of the (3+1)D fluid dynamical model, but it is also seen in UrQMD [17].

At high energy collisions, we need an initial state model, which describes the dynamics until local equilibration is reached. There are several options for describing this pre-equilibrium dynamics, using color glass condensate (CGC) fields, parton (or hadron) kinetic theory, or one-dimensional Yang-Mills field (or flux tube) models [1,2]. In the (3+1)D PICR fluid dynamical model that we use as our guidance for the FD development, this last choice is used.

It is important to mention that for peripheral collisions the initial shear and sometimes even the angular momentum are neglected, while realistic initial state models include these features [5,6,17].

From the initial shear flow, in the (3+1)D PICR fluid dynamical model the general rotation develops gradually in 1–2 fm/c time. Thus, the Exact model is applicable from this point of time on [12]. At the energies we discuss, by this time the matter is in the locally equilibrated QGP phase, and the local vorticity develops also. Because of the spin-orbit interaction the local vorticity and the spin of quarks equilibrate. The essential part of the dynamical development of flow (and other collective mechanical processes) takes place in the QGP phase, which is indicated by the constituent quark number scaling of the flow harmonics.

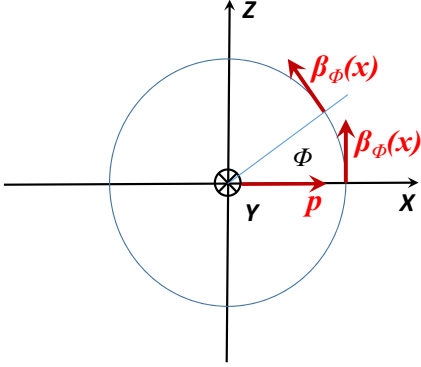


FIG. 1. (Color online) The direction of axes, as well as the momentum  $p$ , and flow  $\beta$  vectors. The azimuth angle is measured from the direction of the  $p$  vector, i.e., from the  $x$  axis.

This most significant middle stage of the reaction can be modeled by the “Exact” model [11]. The model is based on a set of scaling variables,

$$(s_r, s_y) = \left( \frac{x^2 + z^2}{R^2}, \frac{y^2}{Y^2} \right), \quad (1)$$

in terms of the transverse and axial coordinates,  $x$ ,  $z$ , and  $y$ , and the characteristic radius  $R$  and axial length  $Y$  parameters. The scaling parameter  $s = s_r + s_y$  is also introduced, being the scaling variable as it appears in the thermodynamical relations. Here we have interchanged the  $y$  and  $z$  axes to resonate with choice of axes in heavy ion collision literature, in which the reaction plane, in which the system rotates, is spanned by  $e_x$  and  $e_z$ , leaving the axis of rotation to be defined by  $e_y$ .

Reference [12] calibrates the parameters of the Exact model to the (3+1)D fluid dynamical model. The parameters are extracted for experiments at  $\sqrt{S_{NN}} = 2.76A$  TeV with impact parameter  $b = 0.7b_{\text{Max}}$  (see Figs. 1 and 2). In the (3+1)D PICR model, rotation may increase because of Kelvin-Helmholtz instability, whereas in the Exact model—and the later stages in the experiments themselves—rotation slows because of a transfer of energy to the explosively increasing radial expansion of the system. The Exact model, therefore, is suited to describe the period from the equilibration of rotation up to the freeze-out.

In [11] the solution for a flow of conserved number density, together with a constant, temperature-independent compressibility, and a velocity field is described. Hence the solutions take form, in cylindrical coordinates  $(r, y, \phi)$ , where  $r = \sqrt{x^2 + z^2}$  with an equation of motion,  $\dot{r}(t) = v(r, t)$ . The Exact model assumes a linear velocity profile both in the radial  $r$ , and in the axial  $y$  directions. This leads to a flow development where a fluid element starting from a point  $(r_0, y_0, \phi_0)$ , and at

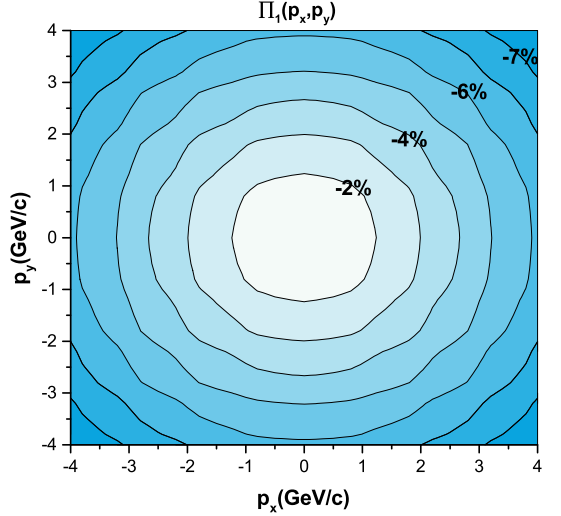


FIG. 2. (Color online) The polarization of  $\Lambda$  particles  $\Pi_1(p)$ , in the participant center-of-mass (c.m.) frame for the first term containing the  $(\nabla \times \beta)$  contribution, at time  $t = 0.5$  fm/c after the equilibration of the rotation, in the Exact model. The polarization  $\Pi_1(p)$  points into the  $-y$  direction and changes from  $-1.5\%$  at the c.m. momentum  $(p_x = p_y = 0)$ , to  $-8\%$  in the corners, in 1% steps per contour line. The negative percentage indicates that the polarization is in the  $-y$  direction. The structure is just like that of the energy weighted vorticity. Because of azimuthal symmetry of the Exact model the  $p_x$  and  $p_z$  dependencies of  $\Pi$  are the same.

a later time  $t$  reaches the point,

$$\begin{aligned} r(t) &= r_0 \frac{R(t)}{R(t_0)}, \\ y(t) &= y_0 \frac{Y(t)}{Y(t_0)}, \\ \phi(t) &= \phi_0 + \int dt \omega(t), \end{aligned} \quad (2)$$

showing explicitly how the solutions evolve in time, rotating and expanding fluid. These equations follow the time evolution of the scaling variables in the radial and axial directions. This is a cylindrically symmetric setup with  $X(t) = Z(t)$ ,  $\sqrt{X^2(t) + Z^2(t)} = R(t)$  and, in general,  $Y(t) \neq R(t)$ .

We have chosen the  $x, z$  plane as our plane of rotation, with  $y$  being the axis of rotation. Our initial angular momentum, then, points in the negative  $y$  direction, with an absolute value of approximately  $1.45 \times 10^4 \hbar$ . In an attempt to determine new observables, we propose a search for  $\Lambda$  polarization. Although the polarization could be described similarly for all fermions, we chose the  $\Lambda$ s, because it is straightforward to determine its polarization from its decay to  $p$  and  $\pi$  (where the  $p$  is emitted into the direction of the polarization). Actually such an experiment was already performed at RHIC, but the results were averaged for  $\Lambda$  emissions to all azimuths, while we

predict significant polarization for particles emitted in the  $\pm x$  direction in the reaction plane [18].

Our expectation is that this polarization, at least in part, will be able to account for the polarization as observed in peripheral regions in the first 10–15 fm/c following the impact in a heavy ion collision.

To evaluate the polarization in the Exact model we use the parametrization of the Exact model based on the realistic (3+1)D PICR fluid dynamical calculation [12], and use the vorticity calculated in the Exact model with these parameters in Ref. [19].

## II. FREEZE-OUT AND POLARIZATION

Polarization of  $\Lambda$ s was subject to theoretical studies before, both in  $p + p$  and in heavy ion reactions. In single  $p + p$  collisions forward production in small-transverse-momentum fragmentation was theoretically studied and also observed. These reactions did result in much higher polarizations up to about 30% [20].

To apply this approach to heavy ion collisions is a complex theoretical problem because several microscopic processes can contribute to polarization and these can be combined with different hadron formation mechanisms [21,22]. In Ref. [21] it was contemplated that the final heavy ion results are dependent on the hadronization mechanisms, and the effect of the decay products of the polarized hyperons on the  $v_2$  flow harmonics  $v_2$  were studied. Reference [22] has also studied the sensitivity of  $\Lambda$  production on the coalescence or recombination mechanisms of the hadron formation.

As the previous works discussed a wide variety and complexity of the microscopic description of hadronization and the resulting polarization, we have followed a simpler statistical picture, based on some simple assumptions of a dilute gas of particles, on the “Relativistic distribution function for particles with spin at local thermodynamical equilibrium” [23].

This work does not address the mechanisms of hadronization and the change of polarization during this process. It also barely discusses the equilibrium between particle polarization and local rotation in thermal equilibrium for dilute gases. Thus, this approach is primarily applicable to the final hadronic matter.

We follow the same reaction mechanism as used in all (3+1)D PICR publications since 2001. We do not assume a three-stage fluid dynamical process in the QGP phase, mixed phase, and hadronic phase because the fastest adiabatic development in the mixed phase would take 30–50 fm/c [24]. Such a long expansion time would contradict all two-particle correlation measurements showing a size and time span at FO of less than 10 fm. Furthermore it would also contradict the observed constituent quark number scaling and the observed large  $\bar{\Omega}$  abundance. The only way out of these problems is supercooling in the QGP phase, followed by rapid hadronization [25,26], and almost immediate freeze-out.

Thus in the PICR fluid dynamical calculations we discuss exclusively the QGP phase, even for supercooled QGP. Based on the mechanical equilibrium, evidenced by the constituent quark number scaling, we have reason to assume that during

the FD evolution there is ample time to equipartition the local rotation among all degrees of freedom in QGP from the spin-orbit interaction. As this is a strongly interacting form of matter the kinetic approximation as a dilute gas is not necessarily applicable, and the energy momentum and local angular momentum should also be carried by the fields.<sup>1</sup> We have to assume that the rapid hadronization maintains equipartition among all degrees of freedom carrying angular momentum. So, based on this assumption we use the approach of [23].

Actually the same applies the statistical and thermal equilibrium among (most of) the abundances of final hadron species. This can be understood based on the fact that the statistical factors are the same in rapid formation of hadrons as in thermal equilibrium.

We use the same assumptions for the Exact fluid dynamical model as we used for the (3+1)D PICR fluid dynamics. Based on the above, in the Exact model the energy weighted thermal vorticity was calculated [19]. We explored the total energy of the system and the energy of expansion, rotation, and internal energy components and their time dependence. We observed the transfer of energy from rotation to expansion, hence the rotation slows as the system expands until the freeze-out.

According to the quantum-field-theoretical approach [23], the expectation value of  $\Lambda$  polarization in an inverse temperature field,  $\beta^\mu(x) = u^\mu(x)/T(x)$ , is

$$\langle \Pi_\mu(x, p) \rangle = \frac{1}{8} \epsilon_{\mu\rho\sigma\tau} (1 - n_F) \partial^\rho \beta^\sigma(x) \frac{p^\tau}{m}, \quad (3)$$

where  $\epsilon_{\mu\rho\sigma\tau}$  is the completely antisymmetric Levi-Civita symbol,  $n_F$  is the Fermi-Jüttner distribution for spin-1/2 particles [ $(1 - n_F)$  is the Pauli blocking factor], and  $p$  is the  $\Lambda$  four-momentum. We integrate this over some volume, and ultimately over all of space, weighted by the number density, normalized by the number of particles in that volume, leaving a momentum-dependent polarization four-vector in the participant frame of reference,

$$\Pi_\mu(p) = \frac{\hbar \epsilon_{\mu\rho\sigma\tau}}{8m} \frac{p^\tau \int d\Sigma_\lambda p^\lambda n_F(x, p) (1 - n_F(x, p)) \partial^\rho \beta^\sigma}{\int d\Sigma_\lambda p^\lambda n_F(x, p)}. \quad (4)$$

Note that, as opposed to electromagnetic phenomena, in which particle and antiparticle will have antialigned polarization vectors, here it is shown that  $\Lambda$  and  $\bar{\Lambda}$  polarizations are aligned in vorticious thermal flow fields.

While the average values of polarization may be as low as 1%–2%, consistent with RHIC bounds, in some regions of momentum space we see a larger polarization, about 5% for momenta in the transverse plane and up to a momentum of 3 GeV/c. Kelvin-Helmholtz instabilities may further enhance rotation, hence the thermal vorticity, defined as

$$\bar{\omega}_{\mu\nu}(x) = \frac{1}{2} (\partial_\nu \beta_\mu - \partial_\mu \beta_\nu), \quad (5)$$

<sup>1</sup>If we would consider only three valence quarks in kinetic equilibrium according to [23], then the polarization of a coalesced baryon would be  $\Pi_B \sim (\Pi_q)^3$ , which would not be measurable.

XIE, GLASTAD, AND CSERNAI

PHYSICAL REVIEW C **92**, 064901 (2015)

and thereby the signal strength increases by 10%–20%. At LHC energies, there may be 5%  $\Lambda$  polarization from the corona effect, single nucleon-nucleon collisions occurring outside of the reaction zone of the collision itself. So attempts should be made to further the understanding of this background, and remove it from measurements to further isolate the  $\Lambda$  polarization as it arises from the collision itself.

The  $\Lambda$  polarization is determined by measuring the angular distribution of the decay protons in the  $\Lambda$ 's rest frame. In this frame the  $\Lambda$  polarization is  $\Pi_0(\mathbf{p})$ , which can be obtained by Lorentz boosting the polarization  $\Pi(\mathbf{p})$  from the participant frame to the  $\Lambda$ 's rest frame [18],

$$\Pi_0(\mathbf{p}) = \Pi(\mathbf{p}) - \frac{\mathbf{p}}{p^0(p^0 + m)} \Pi(\mathbf{p}) \cdot \mathbf{p}, \quad (6)$$

where  $(p^0, \mathbf{p})$  is the  $\Lambda$ 's four-momentum and  $m$  its mass.

Based on this equation we see that to maximize polarization, we need to choose momenta for the  $\Lambda$  such that they lie in the reaction plane, hence we fix  $\mathbf{p}$  in the positive  $x$  direction.

### III. SOLUTION FOR THE $\Lambda$ POLARIZATION

As the  $\Lambda$  is transversely polarized,  $\Pi^\mu p_\mu = 0$ , one can confine himself to the spatial part of  $\Pi^\mu$ . The simplified spatial part of the polarization vector is

$$\begin{aligned} \Pi(\mathbf{p}) = & \frac{\hbar\epsilon}{8m} \frac{\int dV n_F(x, \mathbf{p}) (\nabla \times \boldsymbol{\beta})}{\int dV n_F(x, \mathbf{p})} \\ & + \frac{\hbar\mathbf{p}}{8m} \times \frac{\int dV n_F(x, \mathbf{p}) (\partial_t \boldsymbol{\beta} + \nabla \beta^0)}{\int dV n_F(x, \mathbf{p})}, \quad (7) \end{aligned}$$

where  $n_F(x, \mathbf{p})$  is the phase space distribution of the  $\Lambda$ s. In a previous calculation [18], the  $\mathbf{p}$  dependence of  $n_F$ , was considered negligible in the integral and the time derivative and gradient terms were also assumed to be smaller. The present calculation shows that in general these terms are not negligible and which terms are dominant depends on the particular conditions.

We adopt the parametrization of the model from Ref. [19], with the initial conditions  $R_0 = 2.5$  fm,  $Y_0 = 4.0$  fm,  $R_0 = 0.20$  c,  $\dot{Y}_0 = 0.25$  c,  $\omega_0 = 0.1$  c/fm,  $\kappa = 3/2$ ,  $T_0 = 300$  MeV. For this configuration  $E_{\text{tot}} = 576$  MeV/nucleon.

#### A. The denominator

We first perform the integral in the denominator:

$$A(p) \equiv \int dV n_F = \int_0^R r dr \int_{-Y}^{+Y} dy \int_0^{2\pi} d\phi n_F(x, \mathbf{p}). \quad (8)$$

According to Eq. (3) in Ref. [19] in terms of the scaling variable  $s$ , we have

$$\begin{aligned} n &= n_0 \frac{V_0}{V} \nu(s), \quad (9) \\ \nu(s) &= \frac{1}{\tau(s)} \exp\left(-\frac{1}{2} \int_0^s \frac{du}{\tau(u)}\right) \\ &= 1 \times \exp\left(-\frac{1}{2} \int_0^s du\right), \quad (10) \end{aligned}$$

where the simplifying choice of  $\tau(s) = 1$  is used in the last step. Therefore,

$$n(s) = n_0 \frac{V_0}{V} e^{-\frac{1}{2}s}. \quad (11)$$

The EoS is assumed to be  $\epsilon(s) = \kappa T(t)n(s)$  and the energy density  $\epsilon(s)$  is calculated as in Eq. (29) in Ref. [19], therefore,

$$n(s) = \frac{\epsilon}{\kappa T(t)} = \frac{C_N}{\kappa T} e^{-\frac{sy}{2}} e^{-\frac{sp}{2}}, \quad (12)$$

where  $C_N = \kappa n_0 T_0 \left(\frac{V_0}{V}\right)^{1+1/\kappa}$ .

From Ref. [18], the Fermi-Jüttner distribution is

$$n_F(x, \mathbf{p}) = \frac{1}{e^{p^\mu \beta_\mu - \xi} + 1} \approx \frac{1}{e^{p^\mu \beta_\mu - \xi}} = \frac{e^{\mu/T}}{e^{p^\mu \beta_\mu}}, \quad (13)$$

where the  $\xi = \mu/T$ , and  $\mu$  is the chemical potential. The thermal flow velocity,  $\beta^\mu(x) \equiv u^\mu(x)/T$ , is different at different space-time points  $x$ .

The invariant scalar density for the Jüttner distribution is

$$n = \frac{4\pi m^2 K_2(m/T)}{(2\pi\hbar)^3} e^{\mu/T} = \frac{e^{\mu/T}}{C_0}, \quad (14)$$

where the  $C_0^{-1} = 4\pi m^2 T K_2(m/T)/(2\pi\hbar)^3$ . With  $C_0$  and  $n(s) = n$ , the Fermi-Jüttner distribution can be written as

$$n_F(x, \mathbf{p}) = \frac{e^{\mu/T}}{e^{p^\mu \beta_\mu}} = \frac{C_0 n(s)}{e^{p^\mu \beta_\mu}}. \quad (15)$$

Now we introduce cylindrical coordinates for the location in the configuration space  $x = (r, y, \phi)$ , and using the scaling expansion model [11,12] with the scaling variables  $s, s_r, s_y$ . Now, substituting Eqs. (12) and (15) into the denominator of  $\Pi(\mathbf{p})$ , and parametrizing the range of integrations as in [19] one obtains

$$\begin{aligned} A(p) = & \frac{C_N C_0}{\kappa T} \int_{-aY}^{+aY} dy \exp\left(-\frac{y^2}{2Y^2}\right) \int_0^{bR} r dr \exp\left(-\frac{r^2}{2R^2}\right) \\ & \times \int_0^{2\pi} d\phi e^{-p^\mu \beta_\mu}. \quad (16) \end{aligned}$$

The scalar product in cylindrical coordinates takes the form  $p^\mu \beta_\mu = (p^0, \mathbf{p})(\beta_0, \boldsymbol{\beta}) = p^0 \beta_0 - \mathbf{p} \cdot \boldsymbol{\beta} = p^0 \beta_0 - p_r \beta_r - p_y \beta_y - p_\phi \beta_\phi$ .

In our integral the  $p^\mu$  is given or ‘‘fixed’’ as the argument of  $\Pi(\mathbf{p})$ , while the  $\boldsymbol{\beta} = \boldsymbol{\beta}(x)$  is changing. The integration with respect to  $\phi$  starts from the direction of the  $\mathbf{p}$  vector. According to the Eq. (5) in [19],

$\mathbf{v} = v_r \mathbf{e}_r + v_\phi \mathbf{e}_\phi + v_y \mathbf{e}_y = \frac{\dot{R}}{R} r \mathbf{e}_r + \omega r \mathbf{e}_\phi + \dot{Y} \mathbf{e}_y$ , and  $\boldsymbol{\beta} = \mathbf{u}^\dagger/T = \gamma \mathbf{v}/T$ . Thus in the integral for  $\phi$  we exploit the fact that in the Exact model the radial  $r$ , and axial  $y$  components of the thermal velocity  $\boldsymbol{\beta}$  do not depend on  $\phi$ , while the tangential component does not depend on  $y$ , i.e.,  $\beta_\phi = \gamma r \omega/T$ , but its direction is changing with respect to the direction of  $\mathbf{p}$ . As the integral is over the whole  $2\pi$  angle we can start it at any point of  $\phi$ , so we start it from the externally given  $\mathbf{p}$  direction. Consequently, with this choice of the  $x$  axis,  $\mathbf{p} = (p_r, p_y, 0)$ , and  $p_z = p_\phi = 0$ . In this azimuthally symmetric, exact model it is sufficient to calculate  $\Pi(\mathbf{p})$  for one direction of  $\mathbf{p}$  in the  $[x, z]$  plane.

The direction of the thermal flow velocity  $\boldsymbol{\beta}$  is tangential to the direction  $\phi$ , i.e., it points to the  $\mathbf{e}_{\phi+\pi/2}$  direction. Thus the scalar product is

$$\mathbf{p} \cdot \boldsymbol{\beta}(r, y, \phi) = |p_x| \beta_r \cos(\phi) + p_y \beta_y + |p_x| \beta_\phi \cos\left(\phi + \frac{\pi}{2}\right),$$

where  $\phi$  is the azimuth angle of the position around the  $y$  rotation axis, counted starting from the  $x$  axis. See Fig. 1.

So, inserting the last expression for  $p^\mu \beta_\mu$  into the last term of the integral Eq. (16), the integral with respect to  $\phi$  will take the form,

$$\int_0^{2\pi} d\phi e^{-p^\mu \beta_\mu} = \int_{-\pi}^{\pi} d\phi e^{a \cos(\phi) - b \sin(\phi)} = 2\pi I_0(\sqrt{a^2 + b^2}), \quad (17)$$

where  $a = |p_x| \beta_r = |p_x| \gamma \dot{R} r / TR$  and  $b = |p_x| \beta_\phi = |p_x| \gamma r \omega / T$ , and we used integral No. 3.338(4) in [27]. If we define

$$c_3 = \sqrt{\left(\frac{p_x \gamma \dot{R}}{TR}\right)^2 + \left(\frac{p_x \gamma \omega}{T}\right)^2} = \frac{|p_x| \gamma}{T} \sqrt{(\dot{R}/R)^2 + \omega^2},$$

then  $\sqrt{a^2 + b^2} = c_3 r$ , and

$$\int_0^{2\pi} d\phi e^{-p^\mu \beta_\mu} = e^{-\gamma p^0 / T} e^{p_y \beta_y} \times 2\pi I_0(c_3 r). \quad (18)$$

Now, substituting this back into Eq. (16),

$$\begin{aligned} A(p) &= \int dV n_F(p, s) \\ &= \frac{C_N C_0}{\kappa T} \int_{-aY}^{aY} dr_y \int_0^{bR} r dr \exp\left(-\frac{y^2}{2Y^2} - \frac{r^2}{2R^2}\right) \\ &\quad \times e^{-\gamma p^0 / T} e^{p_y \beta_y} 2\pi I_0(c_3 r). \end{aligned} \quad (19)$$

Now we may use the same simplifying nonrelativistic assumption as in Eq. (5) of Ref. [19], i.e., we approximate  $u^\mu$  by  $v^\mu$  as  $\mathbf{v} = v_r \mathbf{e}_r + v_y \mathbf{e}_y + v_\phi \mathbf{e}_\phi = \frac{\dot{R}}{R} r \mathbf{e}_r + \frac{\dot{Y}}{Y} y \mathbf{e}_y + \omega r \mathbf{e}_\phi$ , and thus  $\gamma = 1$ . It follows, then,

$$\begin{aligned} A(p) &= \int dV n_F(p, s) \\ &= \frac{C_N C_0}{\kappa T} 2\pi e^{-p^0 / T} \int_{-aY}^{aY} \exp(c_1 y - c_2 y^2) dy \\ &\quad \times \int_0^{bR} r I_0(c_3 r) \exp(-c_4 r^2) dr, \end{aligned} \quad (20)$$

where  $c_1 = p_y \dot{Y} / (YT)$ ,  $c_2 = 1/(2Y^2)$ ,  $c_4 = 1/(2R^2)$  are constants.

Now we assume an infinite system with scaling Gaussian density profile, so that the integrals are evaluated up to infinity, i.e., the parameters  $a = \infty$ ,  $b = \infty$ . Thus, the  $y$  component integration in Eq. (20) is calculated as

$$\int_{-\infty}^{+\infty} e^{c_1 y - c_2 y^2} dy = \sqrt{\frac{\pi}{c_2}} \exp\left(\frac{c_1^2}{4c_2}\right), \quad (21)$$

where we used the integral formula No. 2.33(1) in [27], and  $\text{erf}(+\infty) = 1$ ,  $\text{erf}(-\infty) = -1$ .

For the integration of the  $r$  component,

$$\begin{aligned} &\int_0^{+\infty} r I_0(c_3 r) e^{-c_4 r^2} dr \\ &= \frac{1}{c_3 \sqrt{c_4}} \exp\left(\frac{c_3^2}{8c_4}\right) M_{-\frac{1}{2}, 0}\left(\frac{c_3^2}{4c_4}\right), \end{aligned} \quad (22)$$

where the  $M_{-\mu, \nu}(z)$  is the so-called ‘‘Whittaker Function,’’ No. 6.643(2) in [27].

Now, we obtain the final form of Eq. (21):

$$\begin{aligned} A(p) &= \frac{2\pi \sqrt{\pi}}{\kappa T} \frac{C_N C_0}{c_3 \sqrt{c_2 c_4}} e^{-p^0 / T} \exp\left(\frac{c_1^2}{4c_2}\right) \\ &\quad \times \exp\left(\frac{c_3^2}{8c_4}\right) M_{-\frac{1}{2}, 0}\left(\frac{c_3^2}{4c_4}\right). \end{aligned} \quad (23)$$

However, in the relativistic case, the integrations with respect to  $y$  and  $r$  cannot be performed analytically, because of the presence of the factor  $\gamma = 1/\sqrt{1 - v_r^2 - v_y^2 - v_\phi^2}$ .

## B. The numerator

Reference [19] calculates the energy weighted vorticity, which is azimuthally symmetric, i.e., independent of the azimuthal angle  $\phi$ . In the definition of the polarization, Eq. (7), we have  $p^0 n_F(p, x) = \epsilon n_F(p, x)$  for  $\Lambda$ s with momentum  $p$ . In [19], however, the energy weighting is performed with the total energy density of the fluid  $E_{\text{tot}} = E_{\text{int}} + E_{\text{kin}}$ , which in general is not the same as  $\epsilon n_F(p, x)$ . On the other hand the bare vorticity is just a constant in the nonrelativistic Exact model, while the EoS may be more general and it may lead to more involved  $R(t)$  and  $Y(t)$  dependence than the ideal Jüttner gas approximation would allow.

Thus we use the direct, nonrelativistic vorticity values  $\omega(t)$  from Ref. [19], and not the presented energy weighted vorticity, i.e.,

$$\nabla \times \boldsymbol{\beta} = -2\omega(t) \mathbf{e}_y / T(t), \quad (24)$$

so that the thermal vorticity has only the  $y$ -directed component in the Exact model. With the model parameters mentioned above (beginning of Sec. III), the thermal vorticity is  $\hbar(\nabla \times \boldsymbol{\beta}) = -0.13$  at  $t = 0.5$  fm/c, and it decreases very slowly with time, about 1%–2% per 1 fm/c. This constant vorticity will make the numerator simple:

$$B(p) \equiv \int dV n_F(\nabla \times \boldsymbol{\beta}) = \frac{-2\omega \mathbf{e}_y}{T} \times A(p). \quad (25)$$

Therefore, the first term of polarization vector, i.e., Eq. (7) will be

$$\boldsymbol{\Pi}_1(p) = -\frac{\hbar \epsilon}{8m} \frac{\int dV n_F(x, p) (\nabla \times \boldsymbol{\beta})}{\int dV n_F(x, p)} = \frac{\hbar \epsilon \omega}{4mT} \mathbf{e}_y, \quad (26)$$

which means the polarization vector arising from the vorticity  $\boldsymbol{\Pi}_1(p)$  in the Exact rotation model is a constant (although time dependent), and parallel to the  $y$  axis.

One may add the freeze-out (FO) probability to the integral. According to the Ref. [28], the FO probability is  $w_s = (p_\mu \delta_s^\mu)(\mathbf{p} \cdot \mathbf{u}(x))$ , where the approximation is used that

XIE, GLASTAD, AND CSERNAI

PHYSICAL REVIEW C **92**, 064901 (2015)

the FO direction  $\hat{\sigma}_s^\mu$  is parallel to the flow velocity  $\mathbf{u}(x) = \gamma \mathbf{v}(x)$ . In the first term of the numerator, which depends on the constant  $y$ -directed vorticity this FO probability influences the numerator and denominator the same way, so the effect of the two integrals cancel each other in the FO probability also.

### C. The second term

The numerator in the second term of polarization vector reads

$$\mathbf{C}(\mathbf{p}) \equiv \int dV n_F(x, p) (\partial_t \boldsymbol{\beta} + \nabla \beta^0). \quad (27)$$

If, in the nonrelativistic limit,  $\gamma = 1$  is assumed, then  $\nabla \beta^0 = 0$  and  $\partial_t \boldsymbol{\beta} = \partial_t (\mathbf{v}/T)$ , so we have to evaluate only the first term of the sum in the integrand. According to Refs. [19,29], the time derivatives of velocity are

$$\begin{aligned} \partial_t v_r &= \left[ \left( \frac{\ddot{R}}{R} - \frac{\dot{R}^2}{R^2} \right) - \omega^2 \right] r \equiv c_5 r, \\ \partial_t v_\phi &= \left( \dot{\omega} + 2 \frac{\dot{R}}{R} \omega \right) r \equiv c_6 r, \\ \partial_t v_y &= \left[ \frac{\ddot{Y}}{Y} - \frac{\dot{Y}^2}{Y^2} \right] y \equiv c_7 y, \end{aligned} \quad (28)$$

where  $c_5 = (\ddot{R}/R - \dot{R}^2/R^2 - \omega^2)$ ,  $c_6 = (\dot{\omega} + 2(\dot{R}/R)\omega)$ , and  $c_7 = (\ddot{Y}/Y - \dot{Y}^2/Y^2)$ .

Therefore,

$$\partial_t \boldsymbol{\beta} = (c_5 r \mathbf{e}_r + c_6 r \mathbf{e}_\phi + c_7 y \mathbf{e}_y)/T,$$

provides the time components of the vorticity in the three spatial directions. Here, as the model is symmetric,  $\partial_t \beta_y$  vanishes, and with the model parameters mentioned above (Sec. III), at  $t = 0.5$  fm/c and  $r = 1$  fm  $\frac{h}{c} \partial_t \beta_r = 0.024$  and  $\frac{h}{c} \partial_t \beta_\phi = 0.009$ . Both these vorticity components decrease slowly with time by about 0.0005 in 1 fm/c.

Equation (27) is a volume integral of a vectorial quantity, which is not convenient to perform in cylindrical coordinates. So we transform it into Cartesian coordinates:  $\mathbf{e}_r = \cos \phi \mathbf{e}_x + \sin \phi \mathbf{e}_z$ ,  $\mathbf{e}_\phi = -\sin \phi \mathbf{e}_x + \cos \phi \mathbf{e}_z$ . Therefore,  $T \partial_t \boldsymbol{\beta} = (c_5 \cos \phi - c_6 \sin \phi) r \mathbf{e}_x + (c_5 \sin \phi + c_6 \cos \phi) r \mathbf{e}_z + c_7 y \mathbf{e}_y$ .

The integral of Eq. (27) can be expanded as

$$\begin{aligned} \mathbf{C}(\mathbf{p}) &= \int dV n_F(x, p) \partial_t \boldsymbol{\beta} \\ &= \frac{C_N C_0}{\kappa T} e^{-p_0/T} \iiint r dr d\phi dy \exp(c_1 y - c_2 y^2) \\ &\quad \times \exp(a \cos \phi - b \sin \phi - c_4 r^2) \partial_t \boldsymbol{\beta}, \end{aligned} \quad (29)$$

where  $a$  and  $b$  are defined after Eq. (17).

It is convenient to define an integrating operator  $\bar{A}$  as

$$\begin{aligned} \bar{A} &= \int dV n_F(x, p) \times \\ &= \iiint r dr d\phi dy e^{c_1 y - c_2 y^2} e^{a \cos \phi - b \sin \phi - c_4 r^2} \times, \end{aligned}$$

and then Eq. (29) will be

$$\mathbf{C}(\mathbf{p}) = \bar{A} \partial_t \boldsymbol{\beta} \equiv \frac{1}{T} (I \mathbf{e}_x + J \mathbf{e}_z + H \mathbf{e}_y), \quad (30)$$

where we defined

$$\begin{aligned} I &\equiv \bar{A} (c_5 \cos \phi - c_6 \sin \phi) r, \\ J &\equiv \bar{A} (c_5 \sin \phi + c_6 \cos \phi) r, \\ H &\equiv \bar{A} c_7 y. \end{aligned}$$

Using the integral formula No. 2.33(6) of [27] the function  $H$  becomes

$$\begin{aligned} H &= \frac{2\pi \sqrt{\pi} C_N C_0}{\kappa T} e^{-p_0/T} \frac{c_7 c_1}{2c_3 c_2 \sqrt{c_4 c_2}} \\ &\quad \times \exp\left(\frac{c_3^2}{8c_4}\right) \exp\left(\frac{c_1^2}{4c_2^2}\right) M_{-\frac{1}{2}, 0}\left(\frac{c_3^2}{4c_4}\right). \end{aligned} \quad (31)$$

The function  $I$  can be expanded as a function of integrals over  $\phi$ ,  $r$ , and  $y$ . The integral over  $\phi$  brings in the Bessel function,  $2\pi c_8 I_1(c_3 r)/c_3$  [see No. 3.937 (1) and (2) of [27]], where  $c_8 = (c_5 a' - c_6 b')$ ,  $a' = a/r = |p_x| \dot{R}/TR$ , and  $b' = b/r = |p_x| \omega/T$ . Subsequently, the integral with respect to  $r$  brings in the ‘‘Whittaker Function’’ and then the final form of  $I$  after performing the separable integration with respect to  $y$  leads to

$$\begin{aligned} I &= \frac{2\pi \sqrt{\pi} C_N C_0}{\kappa T} e^{-p_0/T} \frac{c_8}{c_3^2 c_4 \sqrt{c_2}} \\ &\quad \times \exp\left(\frac{c_3^2}{8c_4}\right) \exp\left(\frac{c_1^2}{4c_2^2}\right) M_{-1, \frac{1}{2}}\left(\frac{c_3^2}{4c_4}\right). \end{aligned} \quad (32)$$

Evaluating the integral  $J$  is similar to  $I$ :

$$\begin{aligned} J &= \frac{2\pi \sqrt{\pi} C_N C_0}{\kappa T} e^{-p_0/T} \frac{c_9}{c_3^2 c_4 \sqrt{c_2}} \\ &\quad \times \exp\left(\frac{c_3^2}{8c_4}\right) \exp\left(\frac{c_1^2}{4c_2^2}\right) M_{-1, \frac{1}{2}}\left(\frac{c_3^2}{4c_4}\right), \end{aligned} \quad (33)$$

where the only difference is  $c_9 = (c_5 b' + c_6 a')$  compared to  $c_8$  in  $I$ .

Then, substituting  $I$ ,  $J$ ,  $H$  back into Eq. (30), one can obtain the analytical solution for numerator in the second term of the polarization vector as

$$\begin{aligned} \mathbf{C}(\mathbf{p}) &= \int dV n_F(x, p) \partial_t \boldsymbol{\beta} = \frac{1}{T} (I \mathbf{e}_x + J \mathbf{e}_z + H \mathbf{e}_y) \\ &= \frac{2\pi \sqrt{\pi} C_N C_0}{\kappa T^2} e^{-p_0/T} \exp\left(\frac{c_3^2}{8c_4}\right) \exp\left(\frac{c_1^2}{4c_2^2}\right) \\ &\quad \times \left[ \frac{c_8}{c_3^2 c_4 \sqrt{c_2}} M_{-1, \frac{1}{2}}\left(\frac{c_3^2}{4c_4}\right) \mathbf{e}_x \right. \\ &\quad \left. + \frac{c_9}{c_3^2 c_4 \sqrt{c_2}} M_{-1, \frac{1}{2}}\left(\frac{c_3^2}{4c_4}\right) \mathbf{e}_z \right. \\ &\quad \left. + \frac{c_7 c_1}{2c_3 c_2 \sqrt{c_4 c_2}} M_{-\frac{1}{2}, 0}\left(\frac{c_3^2}{4c_4}\right) \mathbf{e}_y \right]. \end{aligned} \quad (34)$$

Dividing this by  $A(\mathbf{p})$ , i.e., Eq. (23), one gets

$$\frac{\mathbf{C}(\mathbf{p})}{A(\mathbf{p})} = \frac{1}{T} \left[ \frac{c_8}{c_3\sqrt{c_4}} \frac{M_{-1,\frac{1}{2}}}{M_{-\frac{1}{2},0}} \mathbf{e}_x + \frac{c_9}{c_3\sqrt{c_4}} \frac{M_{-1,\frac{1}{2}}}{M_{-\frac{1}{2},0}} \mathbf{e}_z + \frac{c_7c_1}{2c_2} \mathbf{e}_y \right]. \quad (35)$$

Then, we obtain the second term of the polarization vector:

$$\begin{aligned} \Pi_2(\mathbf{p}) &= \frac{\hbar\mathbf{p}}{8m} \times \frac{\mathbf{C}(\mathbf{p})}{A(\mathbf{p})} \\ &= \frac{\hbar}{8mT} \left[ \frac{p_y c_9}{c_3\sqrt{c_4}} \frac{M_{-1,\frac{1}{2}}}{M_{-\frac{1}{2},0}} \mathbf{e}_x - \frac{|p_x|c_9}{c_3\sqrt{c_4}} \frac{M_{-1,\frac{1}{2}}}{M_{-\frac{1}{2},0}} \mathbf{e}_y \right. \\ &\quad \left. + \left( \frac{|p_x|c_7c_1}{2c_2} - \frac{p_y c_8}{c_3\sqrt{c_4}} \frac{M_{-1,\frac{1}{2}}}{M_{-\frac{1}{2},0}} \right) \mathbf{e}_z \right]. \quad (36) \end{aligned}$$

As we can see, and as is given also by the definition, Eq. (7), the second term of polarization is orthogonal to the particle momentum:

$$\Pi_2(\mathbf{p}) \perp \mathbf{p}, \quad (37)$$

thus if we use the choice that  $\mathbf{p}$  should be in the  $[x, y]$  plane and its  $z$  component should vanish, then the  $y$  component of  $\Pi_2(\mathbf{p})$ , should depend on  $p_x$  only (see Fig. 5).

#### IV. THE FREEZE-OUT STAGE

The fluid dynamical model is in principle not adequate to describe the final, post-freeze-out (FO) particle distributions, the abundance of the particle species, and also their polarization. This is so because the post-freeze-out distributions must not be in local thermal equilibrium and must not have interactions among the final emitted particles. Furthermore, the emitted particles should not move back into the interacting zone, i.e., towards the pre-FO side of the FO hypersurface. How to handle the freeze-out is described in great detail in [30]. It indicates two ways to handle this process: (i) Consider the post-FO matter as if it has an equation of state (EoS). This is only possible if the post FO EoS is that of a noninteracting ideal gas and the FO hypersurface is timelike. (ii) The other approach is that the post-FO matter is described by a dynamical model with weak and rapidly decreasing interaction, like UrQMD or PACIAE, matched to the QGP fluid on the FO hypersurface. The change at crossing this hypersurface is in general significant, as the pre-FO matter is strongly interacting, supercooled QGP, while the post-FO matter is weakly interacting and has different (usually fewer) degrees of freedom in both situations. The FO across the hypersurface is stronger if the latent heat of the transition is larger.

The precise way to perform this transition is described in [30]. This method is demonstrated in several earlier fluid dynamical model calculations (also using the PICR method) for precision calculations of flow harmonics.

As mentioned in the introduction, at high energies (RHIC and LHC) the constituent quark number scaling and the large strangeness abundance clearly indicate a supercooling and rapid hadronization. Furthermore at these energies the transition is in the crossover domain of the EoS, thus the

expected changes are smaller, and the major part of the FO hypersurface is timelike, which allows one to use ideal gas post-FO distributions, as we do it here using the method of [23]. These are the conditions which make the changes in mechanical parameters (e.g.,  $\mathbf{v}$ ) small at freeze-out while the temperature changes are larger [30].

Thus, just in the case of constituent quark number scaling, we assume that other mechanical processes like mechanical polarization will not significantly change at freeze-out at RHIC and LHC energies. This conclusion is restricted to local thermal and flow equilibrium, and should not apply to some of the microscopic processes, which dominate  $p + p$  reactions.

Also, in the case of freeze-out through spacelike FO hypersurfaces, the mechanical parameters change significantly, the post-FO distribution is far from a thermal distribution (it is a cut-Jüttner or canceling-Jüttner distribution), and thus the conditions of [23] that we use, are not satisfied.

In this connection we may mention that in earlier related publications, previous experimental  $\Lambda$  polarization measurements, which were negative, were discussed. It was pointed out that polarization as measured was averaged for all  $\Lambda$  particle directions. Here, as well as in the previously detailed PICR fluid dynamical calculations, it was emphasized that polarization should be measured after finding event by event the reaction plane and the center of mass of the system. Significant polarization can only be expected for particles emitted in selected directions.

Preliminary experimental polarization studies in the RHIC Beam Energy Scan program along these lines are promising [31], and may lead soon to positive quantitative results. At this point in time the present relatively simpler FO treatment of the model calculations with constant time FO are sufficient, and can be refined when quantitative experimental data are available.

#### A. Conclusion

Finally, adding Eqs. (36) and (26) we get the analytical solution for  $\Lambda$  polarization in the Exact model:

$$\begin{aligned} \Pi(\mathbf{p}) &= \frac{\hbar}{8mT} \left[ \frac{p_y c_9}{c_3\sqrt{c_4}} \frac{M_{-1,\frac{1}{2}}}{M_{-\frac{1}{2},0}} \mathbf{e}_x + \left( 2\epsilon\omega - \frac{|p_x|c_9}{c_3\sqrt{c_4}} \right. \right. \\ &\quad \left. \left. \times \frac{M_{-1,\frac{1}{2}}}{M_{-\frac{1}{2},0}} \right) \mathbf{e}_y + \left( \frac{|p_x|c_7c_1}{2c_2} - \frac{p_y c_8}{c_3\sqrt{c_4}} \frac{M_{-1,\frac{1}{2}}}{M_{-\frac{1}{2},0}} \right) \mathbf{e}_z \right]. \quad (38) \end{aligned}$$

Notice that Eq. (38) is the analytical solution in the nonrelativistic limit. The ‘‘Whittaker Function,’’  $M_{\mu,\nu}(z)$ , is the confluent hypergeometric function. For the relativistic case, the integrations of the  $\Lambda$ -polarization vector cannot be performed analytically, because of the presence of  $\gamma = 1/\sqrt{1 - v_r^2 - v_y^2 - v_\phi^2}$ , which will make the integrations more involved. Thus, a numerical solution for the  $\Lambda$  polarization would be needed.

The effect of vorticity is shown in Fig. 2. The nonrelativistic Exact model can handle reactions with modest energy and modest rotation, so the overall vorticity and the resulting polarization is not too large. Furthermore, the rotation and

XIE, GLASTAD, AND CSERNAI

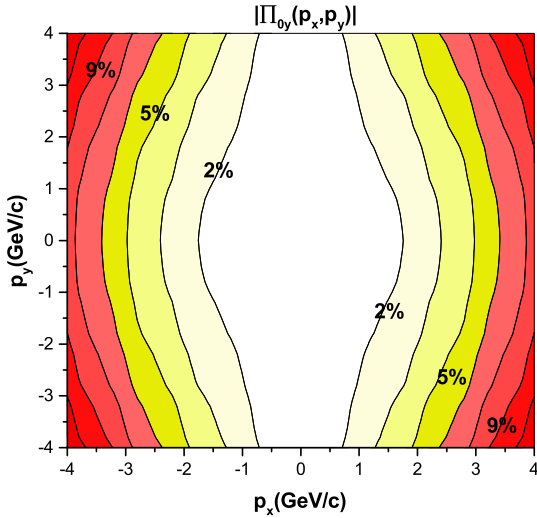
PHYSICAL REVIEW C **92**, 064901 (2015)

FIG. 3. (Color online) The absolute value of  $\Lambda$  polarization,  $\Pi_2(\mathbf{p})$ , in the participant center-of-mass (c.m.) frame for the second term containing the  $(\partial, \beta)$  contribution, at time  $t = 0.5$  fm/c after the equilibration of the rotation, in the Exact model. The polarization changes from zero at the c.m. momentum ( $p_x = p_y = 0$ ), up to 20% in the corners at  $p_x = -4$  GeV/c, in 2.5% steps per contour line. In the corners at  $p_x = 4$  GeV/c, the polarization is 12%. This second term is orthogonal to  $\mathbf{p}$ , and it is smaller, especially at c.m. momenta, where it is negligible. This term arises from the expansion, which is increasing rapidly in the Exact model with time and also increases with the radius. At large radius the larger expansion leads to larger momenta. The structure of the second component of polarization arises from the asymmetries of the different components of  $\Pi_2(\mathbf{p})$ .

vorticity decrease with time while the radial and axial expansion increases. This expansion leads to the second term of polarization  $\Pi_2$ , which depends on  $\partial, \beta$  (while the  $\nabla \beta^0$  terms vanishes in the nonrelativistic approximation). Because of the simplicity of the Exact model, the vorticity arising from the shear flow of the peripheral initial state is constant in space and depends on the time only. However, because of the construction of thermal vorticity, both the angular momentum and the temperature in the denominator decrease with time, thus  $\nabla \times \beta$  is hardly decreasing with the time, and it has a significant value,  $-0.13$ , in natural units. At the same time in this model the time-dependent vorticity is smaller by almost an order of magnitude. The time-dependent vorticity components also decrease faster than the one originating from the initial shear flow.

Nevertheless, the second term in the polarization is of comparable magnitude to the term arising from local vorticity; see Fig. 3.

The presented plots are such that  $p_x$  points into the direction of the observed  $\Lambda$  particle, while the  $p_y$  is the axis direction. All results should be either symmetric or antisymmetric for a  $\pm p_y$  change. On the other hand reversing the  $p_x$  axis must not change the data, as the  $x$  axis is chosen to be the direction of

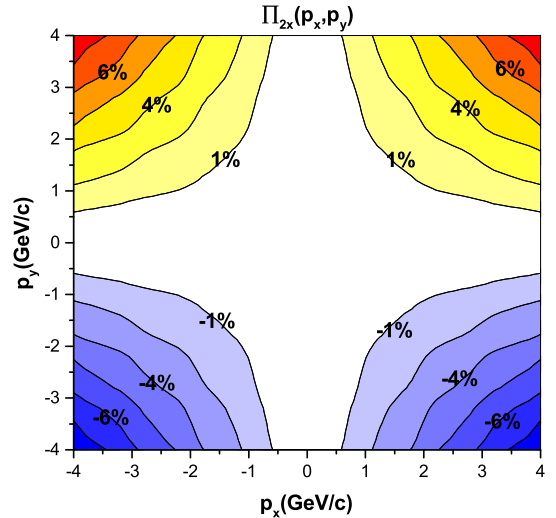


FIG. 4. (Color online) The  $x$  component of the  $\Lambda$  polarization  $\Pi_{2x}(\mathbf{p})$  in the participant center-of-mass (c.m.) frame for the second term containing the  $(\partial, \beta)$  contribution, at time  $t = 0.5$  fm/c after the equilibration of the rotation, in the Exact model. The polarization vanishes at the c.m. momentum ( $p_x = p_y = 0$ ), and changes from zero up or down to  $\pm 8\%$  in the corners, in 1% steps per contour line. This term arises from the expansion, which is increasing rapidly in the Exact model with time and also increases with the radius. At large radius the larger expansion leads to larger momenta.

the argument of  $\Pi(\mathbf{p})$ , which must be azimuthally symmetric in the  $[x, y]$  plane.

The polarization arising from the dynamics of the radial and spherical expansion  $\Pi_2$  was not discussed before in the literature, as the dominance of the vorticity effect was anticipated and studied up to now. The  $\Pi_2$  plots in Figs. 3, 4, 5, and 7 show the components of the polarization arising from the dynamics of the spherical expansion. The most interesting  $y$  component arises from the  $x$  component of the momentum and the  $z$  component of the thermal velocity change  $\beta_z$  (Fig. 5).

Now if we study the axis directed components, this is given by  $\Pi_y = \Pi_{1y} + \Pi_{2y}$ . Both these terms have a negative maxima of the same magnitude ( $-8\%$ ), at the corners  $p_x, p_y = \pm 4$  GeV/c, thus these terms add up constructively and result in  $\Lambda$ -particle polarizations reaching  $-16\%$  at high momenta. At small momenta the polarization is still the same sign but has a reduced value of the order of 1.5% arising from the vorticity (Fig. 6).

In this Exact model the  $x$  and  $z$  components of the polarization arise only from the second term  $\Pi_2(\mathbf{p})$ . The  $x$  component is reaching  $\pm 8\%$ , while the  $z$  component is smaller; it reaches about  $\pm 3\%$ . These both are asymmetric for  $\pm p_y$  change, and show an opposite symmetry. The  $x$  component is proportional to  $p_y$  and the dynamics of radial expansion. Thus it follows the signature of  $p_y$  (Fig. 4). The  $z$  component is proportional to  $p_x$  and the dynamics of radial expansion, thus it follows the signature of  $p_x$  (Fig. 7). The  $z$  component

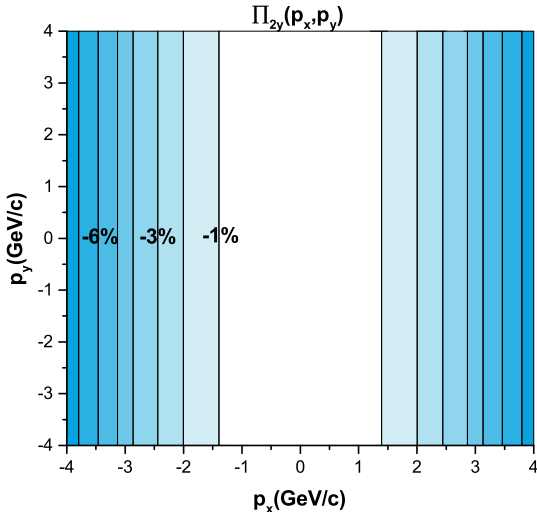


FIG. 5. (Color online) The  $y$  component of  $\Lambda$  polarization  $\Pi_2(\mathbf{p})$ , in the participant center-of-mass (c.m.) frame for the first term containing the  $(\partial_t\beta)$  contribution, at time  $t = 0.5$  fm/c after the equilibration of the rotation, in the Exact model. The polarization changes from zero in the middle to  $-8\%$  at  $p_x = \pm 4$  GeV/c, in 1% steps per contour line. This  $y$ -component points into the axis direction just as the first term  $\Pi_1$ , thus these two are additive. The  $y$  component of  $\Pi_2(\mathbf{p})$  does not depend on  $p_y$ , as shown in Eq. (36).

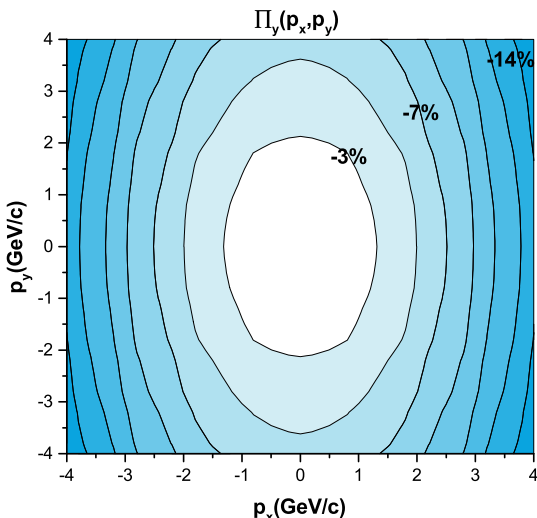


FIG. 6. (Color online) The  $y$  component of  $\Lambda$  polarization  $\Pi(\mathbf{p})$  in the participant center-of-mass (c.m.) frame for the second term containing the  $(\partial_t\beta)$  contribution at time  $t = 0.5$  fm/c after the equilibration of the rotation in the Exact model. The polarization is  $-1.5\%$  at the c.m. momentum ( $p_x = p_y = 0$ ), it is  $-16\%$  in the corners. The change is in steps of 2% per contour line.

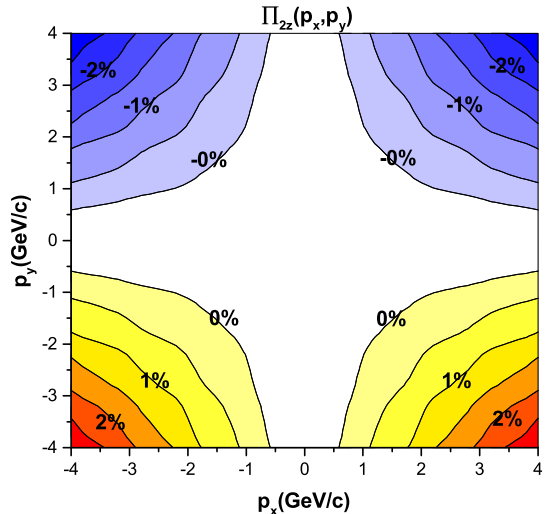


FIG. 7. (Color online) The  $z$  component of  $\Lambda$  polarization  $\Pi_2(\mathbf{p})$  in the participant center-of-mass (c.m.) frame for the second term containing the  $(\partial_t\beta)$  contribution, at time  $t = 0.5$  fm/c after the equilibration of the rotation, in the Exact model. The polarization vanishes at the c.m. momentum ( $p_x = p_y = 0$ ); it is  $\pm 3\%$  in the corners. The change is in steps of 0.5% per contour line. The corners at  $p_y = -4$  GeV/c are positive while at  $p_y = 4$  GeV/c are negative.

is proportional to  $p_x\dot{\beta}_y$  and inversely proportional to  $p_y\dot{\beta}_x$  (Fig. 7). These two effects compensate each other so the maxima of the polarization are smaller and the symmetry is opposite to that of the  $x$  component. This term is sensitive to the balance between the axial expansion and the radial expansion in the model.

The  $\Lambda$  polarization is measured via the angular distribution of the decay protons in the  $\Lambda$ 's rest frame, as shown in Eq. (6). The resulting distribution is shown in Fig. 8. This new study indicates that the dynamics of the expansion may lead to non-negligible contribution to the observable polarization. The structure of  $\Pi_{0y}(\mathbf{p})$  is similar to the one obtained in Ref. [18], but here the contribution of the “second”  $\partial_t\beta$  term is also included, which makes the  $y$ -directed polarization stronger at high  $p_x$  values, 12%, while it was 9% in Ref. [18], both in the negative  $y$  direction. Furthermore, the second term changes the structure, of the momentum dependence of  $\Pi_{0y}(\mathbf{p})$ , and it becomes  $\pm p_x$  asymmetric.

Recently the vorticity and polarization were also studied in two fluid dynamical models [32]. The initial states that were used from Bozek and Gubser neglected fully the initial shear flow in the central domain of the reaction, in contrast to other models where this is present [1,2,17,33,34]. This results in negligible thermal vorticity in the central domain of the collision (Figs. 3 and 13 of Ref. [32]), and consequently a negligible polarization from the vorticity from the “first term” discussed here. Thus, the observed vorticity arises from the “second term.”

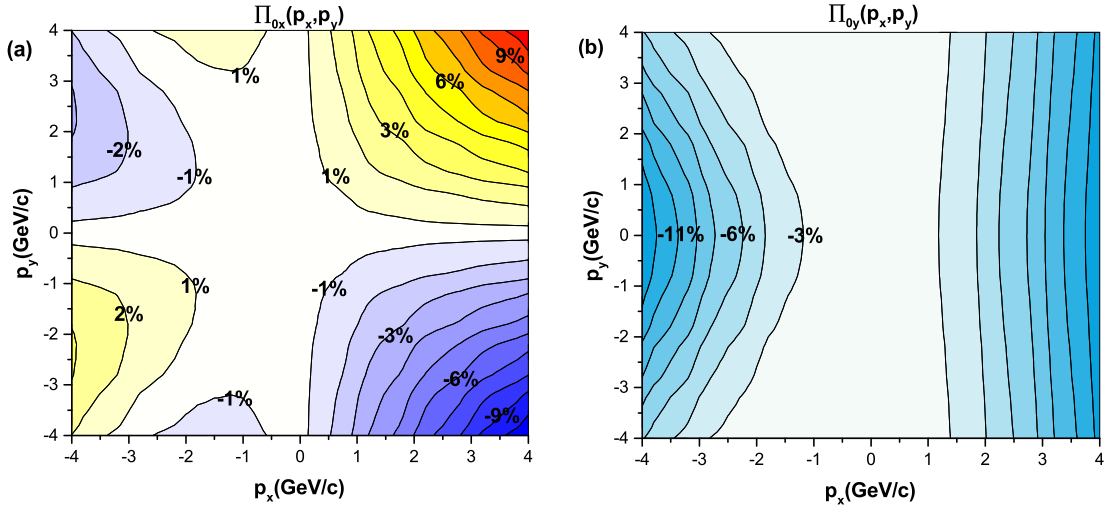


FIG. 8. (Color online) The (a) radial  $x$  and (b) axial  $y$  components of  $\Lambda$  polarization  $\Pi_0(\mathbf{p})$  in the  $\Lambda$ 's rest frame. For  $\Pi_{0x}(\mathbf{p})$  the contours represent changes of 1% from  $-9.5\%$  in the upper left-hand corner to  $9.5\%$  in the upper right-hand corner, whereas the contours of  $\Pi_{0y}(\mathbf{p})$  change in steps of 2% ranging from  $\Pi_{0y} = 0$  (!) at the c.m. momentum ( $p_x = p_y = 0$ ) to  $-12\%$  for  $p_x = \pm 4 \text{ GeV}/c$  at the edges. Both plots are asymmetric because of the Lorentz boost to the  $\Lambda$  rest frame.

On the other hand there is qualitative agreement between Fig. 12 of Ref. [32] and this work in the sense that only the  $y$ -directed (i.e.,  $[x, z]$  or  $[x, \eta]$ ) component of the vorticity leads to an overall average net polarization. This arises in both models from the initial angular momentum and points into the  $-y$  direction. In Ref. [32] this arises as a consequence of viscous evolution of the initial, vorticity-less flow, while in our Exact model it is present in the initial state.

Recent preliminary experimental results reported for the first time [31], significant  $\Lambda$  and  $\bar{\Lambda}$  polarization for peripheral collisions at RHIC for beam energies  $\sqrt{s_{NN}} = 7.7 - 39 \text{ GeV}$  aligned with the axis direction of the angular momentum of the participant system. Furthermore, the  $\Lambda$  and  $\bar{\Lambda}$  polarizations were pointing in the same direction confirming our approach.

In this work we analyzed and compared the two terms of polarization, in the Exact model. Including both rotation and expansion, and vorticity arising from both of these effects enables us to study the consequences of the two terms separately. This study indicates that the assumptions regarding the initial state are influencing the predictions on the observed vorticity, while in all cases observable polarization is predicted.

#### ACKNOWLEDGMENTS

Enlightening discussions with Sharareh Mehrabi Pari, Francesco Becattini, Eirik Hatlen, Istvan Papp, Stuart Holland, and Sindre Velle are gratefully acknowledged. One of the authors, Y.L.X., is supported by the China Scholarship Council.

- 
- [1] V. K. Magas, L. P. Csernai, and D. D. Strottman, *Phys. Rev. C* **64**, 014901 (2001).
  - [2] V. K. Magas, L. P. Csernai, and D. D. Strottman, *Nucl. Phys. A* **712**, 167 (2002).
  - [3] B. McInnes and E. Teo, *Nucl. Phys. B* **878**, 186 (2014).
  - [4] B. McInnes, *Nucl. Phys. B* **887**, 246 (2014).
  - [5] K. Okamoto, C. Nonaka, and Y. Akamatsu, Poster presented at The XXV International Conference on Ultrarelativistic Nucleus-Nucleus Collisions, Sept. 27–Oct. 3, 2015, Kobe, Japan (published electronically).
  - [6] L.-G. Pang, H. Petersen, G.-Y. Qin, V. Roy, and X.-N. Wang, Invited talk presented at The XXV International Conference on Ultrarelativistic Nucleus-Nucleus Collisions, Sept. 27–Oct. 3, 2015, Kobe, Japan (published electronically).
  - [7] L. P. Csernai, W. Greiner, H. Stöcker, I. Tanihata, S. Nagamiya, and J. Knoll, *Phys. Rev. C* **25**, 2482 (1982).
  - [8] L. P. Csernai, G. Fai, and J. Randrup, *Phys. Lett. B* **140**, 149 (1984).
  - [9] L. P. Csernai, V. K. Magas, H. Stöcker, and D. D. Strottman, *Phys. Rev. C* **84**, 024914 (2011).
  - [10] L. P. Csernai, D. D. Strottman, and Cs. Anderlik, *Phys. Rev. C* **85**, 054901 (2012).
  - [11] T. Csörgő and M. I. Nagy, *Phys. Rev. C* **89**, 044901 (2014).
  - [12] L. P. Csernai, D. J. Wang, and T. Csörgő, *Phys. Rev. C* **90**, 024901 (2014).
  - [13] L. P. Csernai and S. Velle, *Int. J. Mod. Phys. E* **23**, 1450043 (2014).

- [14] L. P. Csernai, J. I. Kapusta, and L. D. McLerran, *Phys. Rev. Lett.* **97**, 152303 (2006).
- [15] L. P. Csernai, V. K. Magas, and D. J. Wang, *Phys. Rev. C* **87**, 034906 (2013).
- [16] D. J. Wang, Z. Nédá, and L. P. Csernai, *Phys. Rev. C* **87**, 024908 (2013).
- [17] G. Graef, M. Bleicher, and M. Lisa, *Phys. Rev. C* **89**, 014903 (2014).
- [18] F. Becattini, L. P. Csernai, and D. J. Wang, *Phys. Rev. C* **88**, 034905 (2013).
- [19] L. P. Csernai and J. H. Inderhaug, *Int. J. Mod. Phys. E* **24**, 1550013 (2015).
- [20] T. A. DeGrand and H. I. Miettinen, *Phys. Rev. D* **24**, 2419 (1981).
- [21] Z.-T. Liang and X.-N. Wang, *Phys. Lett. B* **629**, 20 (2005); *Phys. Rev. Lett.* **94**, 102301 (2005).
- [22] A. Ayala, E. Cuautele, G. Herrera, and L. M. Montano, *Phys. Rev. C* **65**, 024902 (2002).
- [23] F. Becattini, V. Chandra, L. Del Zanna, and E. Grossi, *Ann. Phys.* **338**, 32 (2013).
- [24] L. P. Csernai and J. I. Kapusta, *Phys. Rev. D* **46**, 1379 (1992); *Phys. Rev. Lett.* **69**, 737 (1992).
- [25] T. Csörgó and L. P. Csernai, *Phys. Lett. B* **333**, 494 (1994).
- [26] L. P. Csernai and I. N. Mishustin, *Phys. Rev. Lett.* **74**, 5005 (1995).
- [27] I. S. Gradstein and I. M. Ryzhik, *Table of Integrals, Series, and Products* (Academic Press, Waltham, 2007).
- [28] L. P. Csernai, S. Velle, and D. J. Wang, *Phys. Rev. C* **89**, 034916 (2014).
- [29] Horst Stöcker, *Taschenbuch Der Physik* (Harri Deutsch, Frankfurt, 2000).
- [30] Yun Cheng, L. P. Csernai, V. K. Magas, B. R. Schlei, and D. Strottman, *Phys. Rev. C* **81**, 064910 (2010).
- [31] M. A. Lisa, Invited talk at the XI Workshop on Particle Correlations and Femtoscopy (WPCF2015), November 3–7, 2015, Warsaw, Poland.
- [32] F. Becattini, G. Inghirami, V. Rolando, A. Beraudo, L. Del Zanna, A. De Pace, M. Nardi, G. Pagliara, and V. Chandra, *Eur. Phys. J. C* **75**, 406 (2015).
- [33] G.-Y. Chen and R. J. Fries, *Phys. Lett. B* **723**, 417 (2013).
- [34] J. Kapusta, R. J. Fries, G.-Y. Chen, and Y. Li, Invited talk presented at The XXV International Conference on Ultrarelativistic Nucleus-Nucleus Collisions, Sept. 27–Oct. 3, 2015, Kobe, Japan (published electronically).